Percolation effects in the optical properties of Ni-MgO composites

Tae Won Noh, Yi Song, Sung-Ik Lee, and J. R. Gaines
Department of Physics, The Ohio State University, Columbus, Ohio 43210

Hee Dong Park and Eric R. Kreidler
Department of Ceramic Engineering, The Ohio State University, Columbus, Ohio 43210
(Received 22 October 1985)

We prepared Ni-MgO granular metal composites by coprecipitation of NiO-MgO solid solutions and their preferential reduction in a hydrogen atmosphere. These composites have a different topology from that of the granular metal system prepared by cosputtering or coevaporation. The percolation threshold f_c of these Ni-Mgo composites was estimated as 0.32 ± 0.02, which is in good agreement with the prediction of the effective-medium theory (EMT) but much lower than $f_c\approx0.5$ of conventional granular metal films. For each composite with a metal-volume fraction between 0 and 0.4, the reflection spectrum was measured between 20 and 36000 cm^{-1} at room temperature. The detailed comparison of these spectra with the Maxwell-Garnett theory (MGT) and the EMT showed that the Ni-MgO composites were better described by the EMT than by the MGT. The conductivities and the dielectric constants of the composites were derived by a Kramers-Kronig transformation, and they showed a qualitative agreement with the EMT. In the low-frequency region, especially in the far-infrared region, the percolation transition was observed in the reflection spectrum, and also seen in the derived conductivity and the dielectric constant.

I. INTRODUCTION

The optical properties of small-metallic-particle systems have been of interest since the beginning of the century when Maxwell-Garnett[1] provided the first theoretical framework to explain the resonant absorption (or dielectric anomaly) which characterizes such systems. Several types of composites, such as "metallic colloids,"[2] metal "smokes,"[3] discontinuous metallic films,[4] and granular metal films,[5–16] have been studied by previous workers. Among these various types of composites, granular metal films have received considerable attention in part due to their application as solar absorbers[17] and in part due to new theoretical studies.[18–29] Moreover, by using cosputtering or coevaporation, it is easy to produce granular metal films over wide ranges of metal concentration, so that the metal-insulator transition can be studied systematically.[5–7]

This paper describes the optical properties of a new three-dimensional (3D) granular metal system consisting of nearly spherical nickel (Ni) particles and magnesium oxide (MgO). By choosing a completely different method from that used in conventional granular metal systems, we prepared a NiO-MgO solid solution by coprecipitation and preferentially reduced it into a Ni-MgO composite by exposing it to a hydrogen atmosphere. The Ni particles within this composite were relatively large and were easily characterized by a scanning electron microscope. The volume fraction of Ni in the composite was varied from 0% to 40% so the changes in optical properties near the metal-insulator transition could be studied. Depending on the volume fraction of the metal particles, the optical properties of these composites displayed either metallike or insulatorlike behavior. Especially in the low-frequency region, the percolation transition could be easily observed in the reflection spectrum and the optical constants derived from the Kramers-Kronig transformation (KKT) also indicated this transition. The reflection spectrum was compared with both the Maxwell-Garnett theory (MGT) and the effective-medium theory (EMT) and found to agree better with the EMT than with the MGT. The optical constants derived from the KKT were also compared with the EMT.

II. EXPERIMENTAL TECHNIQUE

A. Sample preparation

The series of Ni-MgO composites used here was prepared by a two-step process: preparation of NiO-MgO solid solutions by coprecipitation and their subsequent reduction in a hydrogen atmosphere. To prepare the NiO-MgO solid solutions, preweighed magnesium nitrate hexahydrate [$Mg(NO_3)_2\cdot6H_2O$] and nickel nitrate hexahydrate [$Ni(NO_3)_2\cdot6H_2O$] were dissolved in doubly distilled water to make nitrate solutions. To obtain a homogeneous mixture, these solutions were mixed by a magnetic stirrer for 10 min. By dropping these nitrate solutions into a potassium carbonate (K_2CO_3) solution, we were able to coprecipitate the magnesium carbonate [$MgCO_3$] and nickel carbonate ($NiCO_3$). The reaction was

$$(Ni_xMg_{1-x})(NO_3)_2+K_2CO_3 \rightarrow (Ni_xMg_{1-x})CO_3+2KNO_3 .$$

Since KNO_3 is soluble in water, we were able to isolate the magnesium and nickel carbonates from the potassium nitrate by centrifuging the solution for 10 min at 5000 rpm

with a Beckman J2-21 centrifuge. The solutions (KNO_3 and water) were then discarded and the coprecipitate was washed with doubly distilled water. These centrifuge and washing operations were repeated several times. The coprecipitate was then dried at 100 °C for 24 h before being ground with acetone in a mortar. To remove the volatiles such as CO_2 and to initiate the solid-state reaction $[x\text{NiO}+(1-x)\text{MgO}=(\text{Ni}_x\text{Mg}_{1-x})\text{O}]$, the coprecipitate was calcined for 24 h at 1000 °C. It was then ground for a second time and fired at 1100 °C for 3 h. After this final heat treatment, the NiO-MgO solid solution was ground one more time, dried and stored in tightly capped vials until used to make the composite. Phase identification of this powder by an x-ray diffractometer verified that all phases belonged to NiO-MgO solid solutions.

The solid solution of NiO-MgO powder was compressed at 20 000 psi into a die (1 cm diameter) to form a wafer-shaped pellet. These pellets were dried at 600 °C for 1 h and then sintered at 1600 °C for 1 h. Finally, the pellets were fired in a hydrogen atmosphere at 1200 °C for 1 h to reduce preferentially the nickel oxide to metallic nickel. By measuring the weight loss of each sample, we insured that the NiO was fully reduced. We also changed the firing temperature of the reduction process from 900 to 1200 °C, and the firing time from 10 min to 2 h in order to understand the kinetics, thermodynamics, and mechanisms of the microstructural evolution. The details of these processes and related measurements will be published elsewhere.[30]

B. Sample characterization

The sample characterization was performed by using a JEM 200CX transmission electron microscope (TEM), and a ISI-SX-30 scanning electron microscope (SEM). Due to the relatively large size of particles (typical radius 0.12—0.23 μm), the SEM pictures were usually good enough to provide detailed information on each sample.

SEM pictures of a typical fracture surface are displayed in Fig. 1. These pictures reveal that the Ni particles are nearly spherical. A detailed examination of these pictures also shows that the particle size tends to increase slowly with the volume fraction f of Ni. Using these pictures

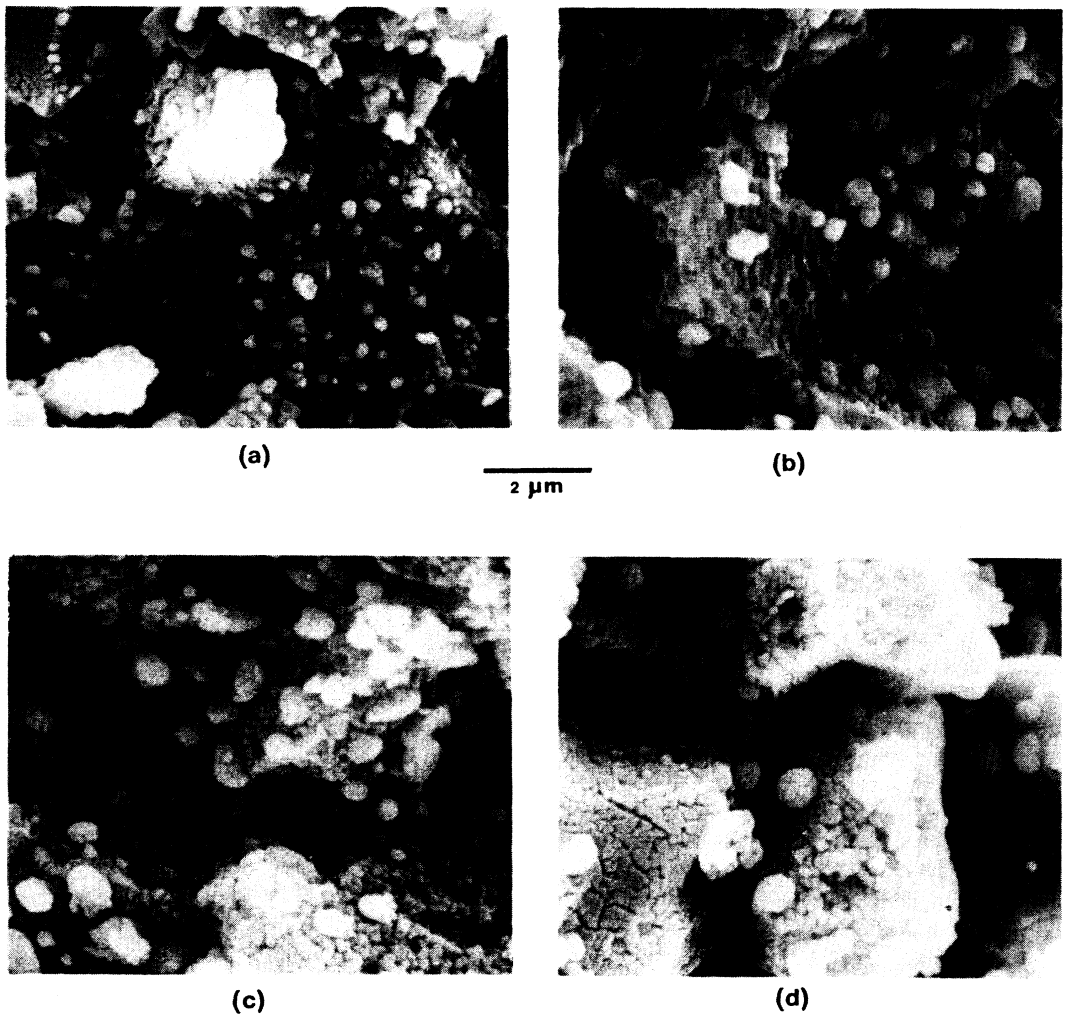

FIG. 1. Scanning electron micrographs of fractured surfaces of the Ni-MgO composites prepared by the coprecipitation of the NiO-MgO solid solutions and their reduction; (a) $f=0.1$, (b) $f=0.2$, (c) $f=0.3$, and (d) $f=0.4$.

and the Carl Zeiss videoplan, we measured the size distribution of the Ni particles. The average radius of the Ni particles measured from these SEM pictures is about 1200 Å for the $f=0.1$ sample, 1800 Å for the $f=0.2$ sample, 2100 Å for the $f=0.3$ sample, and 2300 Å for the $f=0.4$ sample.

One surprising result from these SEM pictures is that little difference exists between the fracture surface for $f=0.4$ and that for $f=0.1$. To understand this puzzle, some SEM pictures of polished surfaces were taken (refer to Fig. 2). The SEM pictures of a polished surface with $f=0.05$, clearly show that Ni particles tend to be located more heavily on the grain boundaries than inside the grain. However, as f increases, the number of particles on the grain boundary does not increase much (as shown in Fig. 1), but the number of particles inside the grain increases very sharply. As f approaches 0.4, there seems to be no distinction between the particle distribution on the grain boundary and inside the grain.

For the TEM measurements, we cut 3-mm-diam disks from the sample pellets, using an ultrasonic cutter. These disks were attached to a Gatan disc grinder with wax and polished until they were about 80 μm thick. Each of these thin disks was then attached to a sample holder and exposed to an Ar beam inside a Gatan ion mill. The Ar beam had a 75° angle of incidence to the sample plane. After about 5 h the angle of the Ar beam was changed to 80° to provide a larger area for the TEM measurement and the sample was exposed to the beam for another 10 h. During this ion-milling process, the sample holder was rotated to provide a uniform exposure of the specimen to the incoming Ar beam.

A typical TEM picture is shown in Fig. 3. This picture shows that some small Ni particles exist which cannot be seen in the SEM pictures. However, since these small particles do not contribute much to the volume fraction of the sample, it was not necessary to include these small particles in the size distribution. In addition, the TEM picture shows that the Ni particles have an almost spherical shape even in a sample with a high-volume fraction ($f=0.3$); in other words, coalescence of Ni particles does not occur even near the metal-insulator transition.

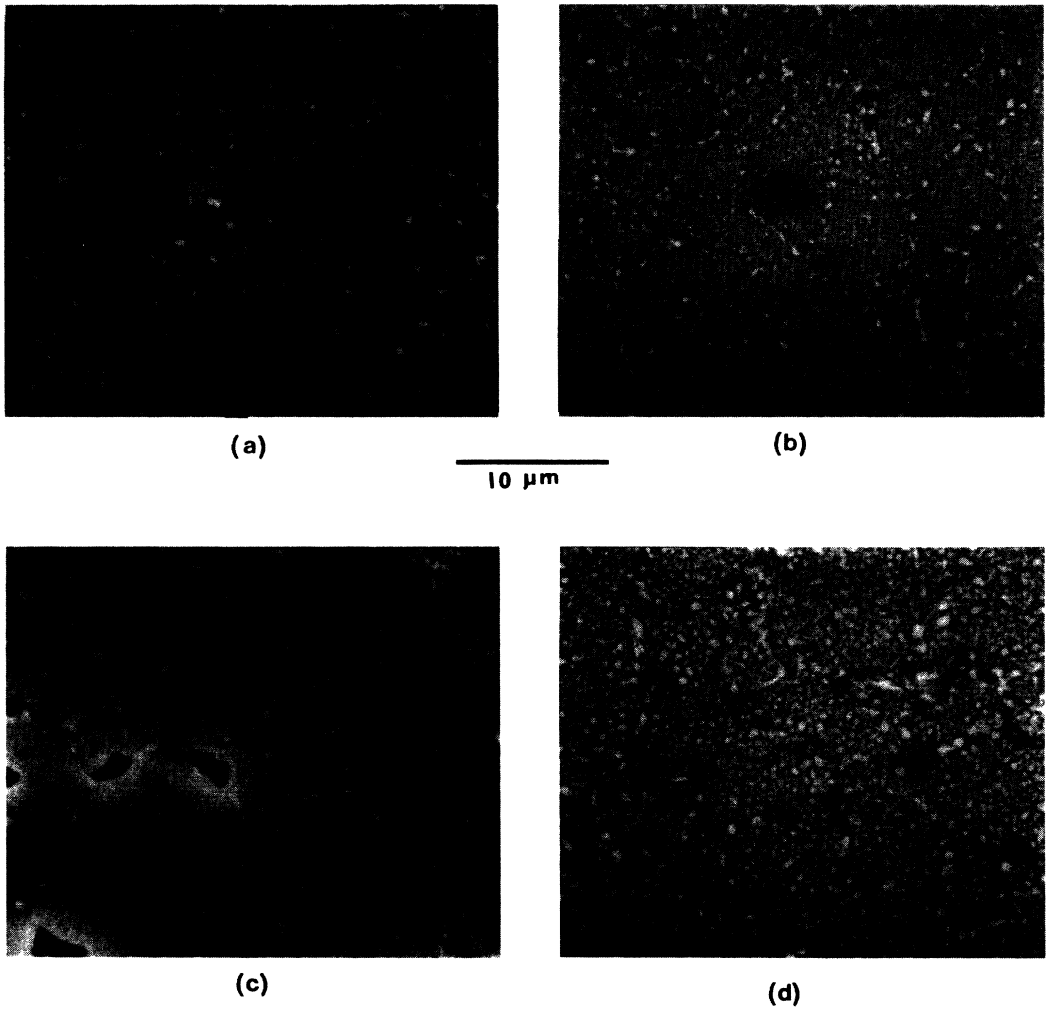

FIG. 2. Scanning electron micrographs of polished surfaces of Ni-MgO composites; (a) $f=0.05$, (b) $f=0.2$, (c) $f=0.3$, and (d) $f=0.4$.

FIG. 3. Transmission electron micrographs of 30% Ni in an MgO sample.

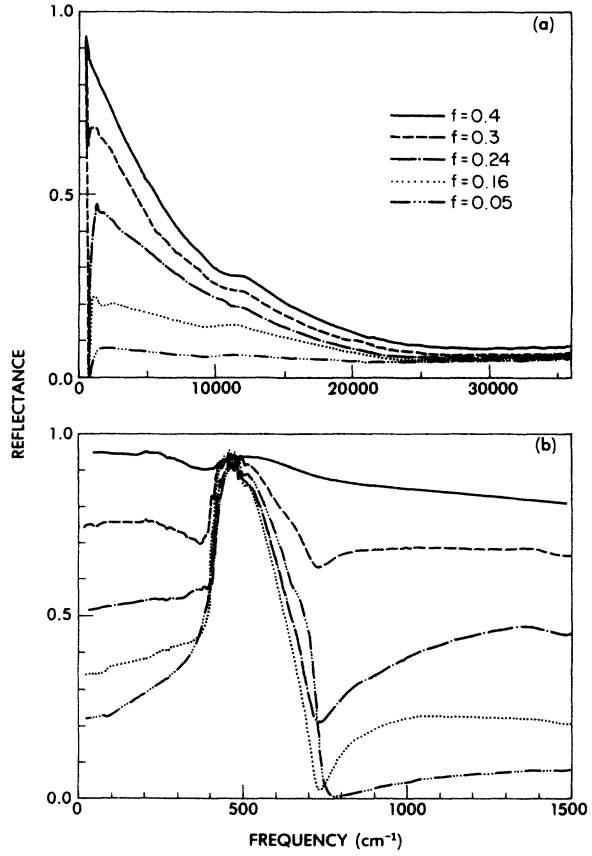

FIG. 4. (a) Measured reflectance between 20 and 36000 cm^{-1} of room-temperature Ni-MgO composites for several volume fractions. The small structures around 11000 cm^{-1} are due to the interband transition of Ni particles. (b) Measured reflectance between 20 and 1500 cm^{-1} of room-temperature Ni-MgO composites. The peaks around 500 cm^{-1} are due to the phonon bands of MgO.

C. Reflectance measurements

The reflection spectrum between 20 and 36000 cm^{-1} was measured at room temperature with a BOMEM DA3.02 Fourier transform spectrophotometer. Four sources, four beam splitters, and five detectors were used to cover the far-infrared, infrared, visible, and ultraviolet regions. All light sources used were unpolarized, and the incident beams entered with an angle of incidence of about 13°.

To obtain accurate reflectance measurements of the samples, one surface had to be smooth and flat. The pellet was ground flat with 600-grit silicon carbide grinding paper and polished using 6 and 1-μm diamond pastes. The samples were wetted with isopropanol throughout the polishing process. Most samples polished by this procedure could be made flat and appeared quite shiny.

Despite the shiny appearance, our samples still showed some effects of diffuse scattering. To compensate for this diffuse scattering, the samples were coated with 3000 Å of Au immediately after the reflectance measurement,[31] and the reflectance of these gold-coated samples was also measured. A comparison between the reflectance from the gold-coated surface and that from the uncoated surface gave a correction for the reflectance due to diffuse scattering. The results of these corrected reflectance measurements are displayed in Fig. 4. The weak structure near 11000 cm^{-1}, shown in Fig. 4(a), is due to the interband transition of Ni. The peaks below 1000 cm^{-1}, indicated in Fig. 4(b), are due to the phonon peaks of MgO. The LO phonon peak located near 640 cm^{-1} can be seen for the $f=0.05$ sample.

III. THEORETICAL CALCULATIONS

A. The dielectric constants of MgO and Ni

Like many other ionic crystals, MgO has pronounced phonon absorption peaks in the far-infrared region. A damped-oscillator model has been frequently used to evaluate the dielectric constant of such ionic crystals. Following Jasperse *et al.*[32] we used the dielectric constant of MgO, ϵ_{MgO}, which was evaluated using a two-resonance damped-oscillator model such that

$$\epsilon_{MgO}=\epsilon_\infty+\sum_{j=1}^{2}\frac{4\pi\rho_i\omega_i^2}{(\omega_j^2-\omega^2)-i\gamma_j\omega}\ , \tag{1}$$

where ϵ_∞ is the high-frequency dielectric constant, $4\pi\rho_j$ the strength, γ_j the damping constant, and ω_j the frequency of the jth resonance. We used the following parameters; $\epsilon_\infty=3.01$, $\omega_1=401$ cm^{-1}, $\omega_2=640$ cm^{-1}, $4\pi\rho_1=6.60$, $4\pi\rho_2=0.045$, $\gamma_1=7.619$ cm^{-1}, and $\gamma_2=102.4$ cm^{-1}. Since the interband transition of MgO starts at a frequency much above 36000 cm^{-1} (the maximum frequency of our measurements), we did not include this interband transition in our calculation.

Ni is a ferromagnetic metal which has optical structures at 0.3 and 1.4 eV.[33] Despite being ferromagnetic, it is generally thought to be a good approximation to assume that the permeability of Ni is that of free space over the wavelength region[33] of our measurements. However, the

structures at 0.3 and 1.4 eV make it difficult to find a proper analytical form of the dielectric constant for Ni, ϵ_{Ni}, since both structures come from interband transitions, not from intraband transitions. The low onset of the interband transition makes it particularly difficult to apply the Drude formula in our measured frequency range. In spite of this difficulty, we still used a Drude expression as suggested by Roverts[34] since no better analytical expression for the dielectric constant of Ni was available. This expression gives ϵ_{Ni}, which is in relatively good agreement with the measured values of ϵ_{Ni} by other workers.[35]

B. The effective dielectric constants

Many physical quantities of inhomogeneous media have been described in terms of an effective dielectric constant, which usually depends on the dielectric constants and the volume fractions of each constituent. The validity of using an effective dielectric constant instead of local dielectric constants depends on two size conditions:[28] First, the inhomogeneities of the medium must be so large that each point in the material can be associated with a macroscopic dielectric constant; secondly, the particle size must be small compared to the wavelength of incident electromagnetic fields. Considering the relatively large size of our Ni particles, only the second condition is of real importance. In the far-infrared and the infrared region where most of the percolation behavior was observed, the second condition is fulfilled. However, above the visible region, the second condition is not satisfied since the size of our particles is then comparable to the wavelength of the incoming beam. Nevertheless, a first-order approximation can still be made.

To evaluate the effective dielectric constant, two different theoretical approaches have been frequently used;[36] the Maxwell-Garnett theory (MGT) (Ref. 1) and the effective-medium theory (EMT) (Refs. 18, 37, and 38). We introduce both theories, with the assumption that the particle shape is spherical.

In the MGT, isolated grains of dielectric constant ϵ_g are embedded in a host material with dielectric constant ϵ_h. The assumption that the grains are isolated within the host is appropriate for low values of the volume fraction f of the grains, leading to an effective dielectric constant, ϵ_{MGT}, given by

$$\epsilon_{MGT}=\epsilon_h+\frac{3\epsilon_h f(\epsilon_g-\epsilon_h)}{(1-f)(\epsilon_g-\epsilon_h)+3\epsilon_h} . \quad (2)$$

Figure 5 is the calculated reflectance of Ni-MgO composites from the MGT treating MgO as a host material (i.e., $\epsilon_g=\epsilon_{Ni}$ and $\epsilon_h=\epsilon_{MgO}$), and Fig. 6 is that from the MGT treating Ni as a host material (i.e., $\epsilon_g=\epsilon_{MgO}$ and $\epsilon_h=\epsilon_{Ni}$). Note that Eq. (2) is inherently asymmetric in the treatment of the two constituents; that is, the transformation of $\epsilon_g \leftrightarrow \epsilon_h$ and $f \leftrightarrow 1-f$ will result in a different effective dielectric constant. In other words, the MGT will give completely different answers for the case of metal grains embedded in an insulating background (Fig. 5) and for insulating grains in a metal background (Fig. 6), even if the volume fraction of metal is the same in the two cases. Note that all curves in Fig. 5 show an insulatorlike

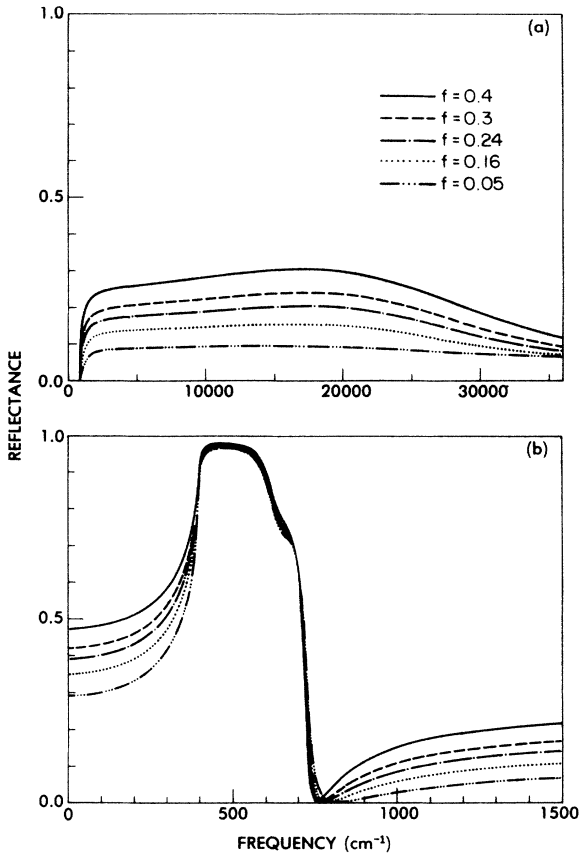

FIG. 5. (a) Reflectance of the Ni-MgO composites calculated by the Maxwell-Garnett theory (MGT) with insulating host. (b) Low-frequency reflectance of the Ni-MgO composites calculated by the MGT with insulating host.

behavior, while all the curves in Fig. 6 show a metal-like behavior. Moreover, *the* MGT *does not predict any percolation transition;* i.e., ϵ_{MGT} varies smoothly from the host value at $f=0$ to the grain value at $f=1$. Despite these shortcomings, the MGT has been applied to numerous metal-insulator composite systems[39] and is generally accepted as a good description of dilute inhomogeneous mixtures.

The EMT is a mean-field theory developed by Bruggeman[37] and generalized by Stroud.[18] According to this theory, individual grains, either metal or insulator, are considered to be embedded in a background (the "effective medium") which has the average properties of the mixture. A self-consistent choice such that the total depolarization field inside the inhomogeneous medium is equal to zero leads to a quadratic equation for the effective dielectric constant ϵ_{EMT},

$$f\frac{\epsilon_{Ni}-\epsilon_{EMT}}{\epsilon_{Ni}+2\epsilon_{EMT}}+(1-f)\frac{\epsilon_{MgO}-\epsilon_{EMT}}{\epsilon_{MgO}+2\epsilon_{EMT}}=0 . \quad (3)$$

Contrary to the MGT, the EMT treats each of the constituents of the medium on an equal basis; in other words, Eq. (3) remains the same for the transformation such as $\epsilon_{Ni} \leftrightarrow \epsilon_{MgO}$ and $f \leftrightarrow (1-f)$. Moreover, *the* EMT *predicts a*

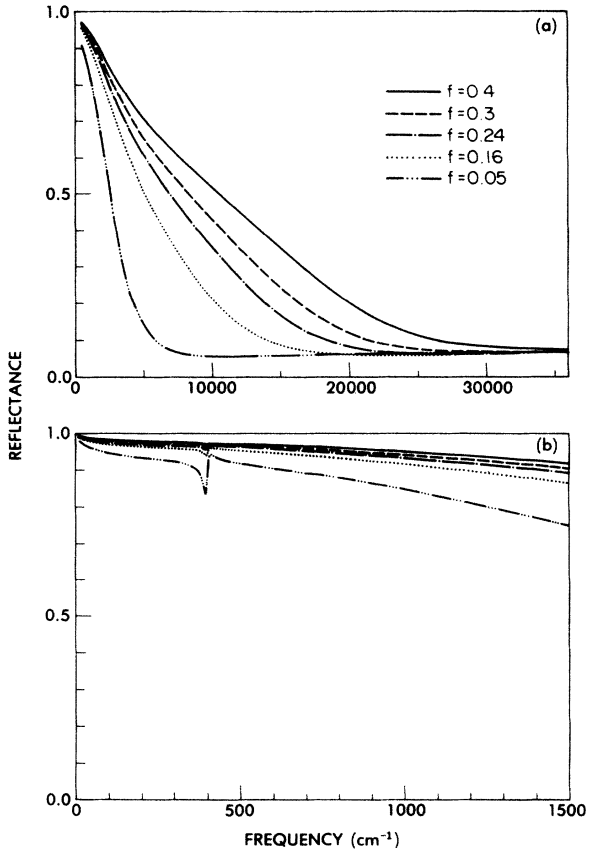

FIG. 6. (a) Calculated reflectance of the Ni-MgO composites using the MGT with metal host. (b) Low-frequency reflectance calculated by the MGT with metal host.

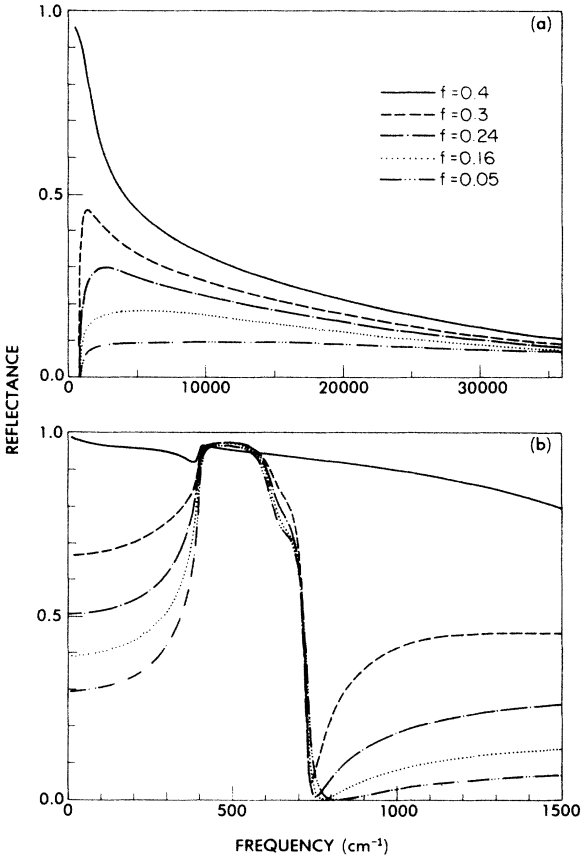

FIG. 7. (a) Calculated reflectance of the Ni-MgO composites using the effective-medium theory (EMT). (b) Low-frequency details of reflectance evaluated by the EMT.

metal-insulator transition at a critical volume fraction $f_c=\frac{1}{3}$ for spherical particles. Therefore, the EMT has been applied by many workers to explain percolation behavior.[18,19,21,23,39]

Figure 7 is the calculated reflectance of Ni-MgO composites using the EMT. Contrary to Figs. 5 and 6, this figure shows the transition from insulatorlike behavior ($f<f_c=\frac{1}{3}$) to metal-like behavior ($f>f_c$). This EMT calculation shows at least a qualitative agreement with the experimental result in Fig. 4. From the comparisons of Figs. 5, 6, and 7 with Fig. 4, it is clear that the EMT is much better than the MGT in describing the measured reflectance of Ni-MgO composites in the high-frequency range as well as in the low-frequency range. The detailed comparison is postponed to Sec. IV.

C. Kramers-Kronig transformation of the data

We performed a Kramers-Kronig transformation of the reflectance to evaluate the values of the optical constants. The Kramers-Kronig integral of the measured values of the reflectance provides the phase shift on reflection.[40] With this phase shift and the measured reflectance, the real part of the dielectric constant, ϵ, and the conductivity, σ, could be obtained.

In the KKT, conventional extrapolation procedures[31] were used. For the samples with $f\leq 0.3$, a constant reflectance between 0 and 20 cm^{-1} was assumed. For the samples with $f>0.3$, it was assumed that they followed (at low frequencies) the Hagen-Reubens relation[41] such that

$$R(\omega)=1-A\omega^{1/2}, \tag{4}$$

where R is the reflectance as a function of frequency and A was chosen to make the relation fit the first few data points. For the frequency above our measurements, we made the same extrapolation for all samples. For frequencies between the last data point (36000 cm^{-1}) and 320000 cm^{-1}, the reflectance was extrapolated as ω^{-s}, with the exponent[33] chosen to be $s=0.9$. Above 320000 cm^{-1} the reflectance was assumed to follow the free-electron behavior, i.e., ω^{-4}.

IV. RESULTS AND DISCUSSION

A. Sample characteristics

As mentioned earlier, our Ni-MgO composites were composed of larger metal particles (radius 0.12–0.23 μm) than the conventionally prepared granular metal system

where the typical size of the metal grains was 50 to several hundred angstroms. Beside the difference in the size of the metal particles, there also existed differences in topology as well as the estimated percolation threshold.

Gibson *et al.*[13] showed that the granular metal films prepared by vacuum deposition techniques have one of two radically different topologies. Granular metal systems which contain amorphous insulators such as SiO_2 or Al_2O_3 have a topology such that composites below f_c are composed of metal grains randomly dispersed and completely surrounded by an amorphous oxide matrix and composites above f_c are composed of oxide matrix grains completely surrounded by metal ("cermet topology"). Most composites having crystalline insulators such as MgO or alkali-halide dielectric components follow a topology such that crystallites of insulator and metal are indistinguishable and interspersed ("aggregate topology").

Our Ni-MgO composites did not have "cermet topology" or "aggregate topology." The SEM pictures in Figs. 1 and 2 showed that our Ni-MgO composites were composed of Ni particles dispersed in crystallites of MgO and that contact between the Ni particles was possible. Moreover, no matrix inversion was observed above f_c for our samples, so our samples did not have the "cermet topology." It was also evident that our Ni-MgO composites did not have the "aggregate topology;" MgO crystallites served as a host material even for $f=0.4$ ($>f_c$) samples [refer to Figs. 1(d) and 2(d)], so the Ni particles were easily distinguishable from the MgO. These topological differences of our Ni-MgO composite from the conventional granular metal films presumably results from the different methods used for sample preparation.

A basic aspect of essentially all granular composites that are prepared by cosputtering or coevaporation techniques is the formation of thin insulating coatings onto the metallic grains during deposition.[5,13] The existence of such stabilizing coatings on metal particles results in the preferential growth of individual grains rather than the establishment of percolation paths, so most of the conventionally prepared granular metal films have high percolation thresholds, for example, $f_c \sim 0.5$ for Au granular films.[13]

As we mentioned earlier, the measurement of the weight loss before and after the reduction process showed that NiO in the solid-state solution was fully reduced. Therefore, our Ni-MgO composites were composed with Ni particles devoid of nickel oxide coating. This lack of the stabilizing coating is probably the reason we have a lower value of f_c. Our dc resistivity measurement showed that the percolation threshold of our samples was about $f=0.30$. Analysis of our optical data also supported this f_c value as discussed later. Recent theoretical percolation studies[42] predict that the percolation threshold of a 3D random composite lies between 0.15—0.18. The value of the percolation threshold for our composites higher than such predictions may come from interactions which produce a higher Ni particle density near the grain boundaries than that inside of the MgO particles for low-volume-fraction samples. Even though f_c obtained from our samples was higher than the theoretical percolation predictions, our value was lower than the experimental value ($f_c \sim 0.5$) for granular metal films. Moreover, our estimated percolation threshold $f_c = 0.32 \pm 0.02$ is in an excellent agreement with the EMT predictions.[18,23]

B. The reflectance of an Ni-MgO composite

Both of the theories, the MGT and the EMT, have been frequently used to explain the optical properties of granular metal films. However, the existing comparisons of these basic theories with the experimental data on conventional granular metal systems gives a confusing picture. According to Gittleman and Abeles,[20] their Ag-SiO_2 sample exhibits better agreement with the MGT than with the EMT. However, comparing some other experimental results with theories, Granqvist[12] argued that the Ag-SiO_2 (Ref. 5), Ni-Al_2O_3 (Ref. 10), and W-MgO (Ref. 9) granular metal films were better described by the MGT than by the EMT, but the Au-MgO system[12] showed better agreement with the EMT. Moreover, a recent study by Yamaguchi *et al.*[16] claimed that the sample of Gittleman and Abeles was unduly influenced by the surface of the sample since the sample was very thin, but that the "well-defined" 3D granular metal systems of Ag-MgF_2 followed the EMT.

By careful studies of the topologies, optical measurements, and comparison with theories, Gibson *et al.*[13] showed that the topology of each granular metal system determined its optical properties. From the experimental data and TEM pictures of the Au-Al_2O_3 and the Au-MgO system, they argued that granular metal composites containing amorphous insulators such as SiO_2 or Al_2O_3, which usually had "cermet topology," behaved as predicted by the MGT, but that most composites having crystalline insulators such as MgO or an alkali halide (which had "aggregate topology") could be described by the EMT after including the oxide coating effect.[19] This classification scheme generally holds good for most of the granular metal systems (with a few exceptions such as W-MgO).

In the remainder of this section, we will show that the reflection spectrum of our Ni-MgO system clearly follows the predictions of the EMT rather than that of the MGT, even though our composites have a different topology from conventional granular metal systems. The modification of the EMT due to the oxide coating on the metal particles,[19] used by Gibson *et al.*[13] is not used in this paper, since our Ni particles are free of oxide coating. Moreover, from a comparison of our measured reflectance in Fig. 4 and the calculated reflectance shown in Fig. 6, it is obvious that the MGT calculation based on a metal background cannot explain the details of our measurements. Therefore, when comparing our results with the MGT, we will consider only the case where the insulator is the background host (see Fig. 5).

The high-frequency reflectance given in Figs. 5(a) and 7(a) shows that the MGT and the EMT predict the same results for a low-volume-fraction sample ($f=0.05$), in good agreement with the measured reflectance [refer to Fig. 4(a)]. However, as f increases, the MGT provides totally different results from our measurement, but the EMT gives at least a qualitative agreement with our measured reflectance. As shown in Fig. 5(a), the MGT gives a

flat response region between 5000 and 20000 cm^{-1} independent of volume fraction. The EMT calculation in Fig. 7(a) shows that the flat response region does not exist for $f \geq 0.16$ and that the reflectance will decrease as the frequency increases. Even though our particle size is not small enough to satisfy the approximation of the EMT, the EMT prediction provides a good qualitative description of the measured values in Fig. 4(a).

The percolation transition is not obvious in the high-frequency region [refer to Figs. 4(a) or 7(a)] but it is more evident in the low-frequency reflectance. As we can see in Fig. 4(b), the reflectance of the $f=0.4$ sample approaches unity as the frequency goes to zero; this is a well-known metal-like behavior; however, all other samples ($f \leq 0.3$) show a flat response below 400 cm^{-1}, which is an insulatorlike behavior. The EMT in Fig. 7(b) clearly shows this percolation transition, but the MGT in Fig. 5(b) does not predict it.

Another interesting result in Fig. 4(b) is that every sample below $f=0.3$ shows a dip following the phonon peaks of MgO, but the sample with $f=0.4$ shows no dip. Moreover, the position of the dip is shifted to lower frequency, as f increases. As can be seen in Fig. 7(b), the EMT predicts the shift of the dip following the phonon peaks even though the predicted reflectance at the dip is much smaller than the measured value. Moreover, the EMT predicts that the dip exists for an $f=0.33$ ($<f_c=\frac{1}{3}$) sample, but that it should suddenly disappear for a sample with $f=0.34$ ($>f_c$). Therefore, all of the gross features observed in the reflection spectra can be explained by the EMT.

C. Optical constants

The optical constants obtained from the KKT also show the percolation transition in the low-frequency region (just like the reflectance measurements). As stated earlier, the MGT cannot predict the percolation transition, so we will compare the optical constants derived from the KKT only with the predictions of the EMT.

The percolation transition is evident in the dielectric constant derived from the KKT. In Fig. 8(a), the dielectric constant at low frequencies is negative for the $f=0.4$ sample; a behavior like that of a metal. Even though the phonon bands screen its behavior, every sample below the percolation threshold had a positive dielectric constant at low frequencies, which is typical of insulatorlike behavior. Moreover, below percolation, the dielectric constant at low frequencies increases as f approaches f_c, in agreement with the percolation theories.[43] Most of the percolation behavior seen in Fig. 8(a) agrees with the predictions of the EMT in Fig. 8(b) except for the $f=0.3$ sample. For this sample, the derived dielectric constant in Fig. 8(a) shows two crossovers when compared with that of the $f=0.24$ sample. To understand this phenomenon, we calculated the dielectric constant near the percolation transition region (refer to Fig. 9). Figure 9 shows that the EMT predicts such crossovers of the dielectric constant for a sample with $f=0.32$ (just below the percolation threshold) and that for a sample with $f=0.3$. This agreement indicates that the percolation threshold of our Ni-MgO composite is just above $f=0.3$.

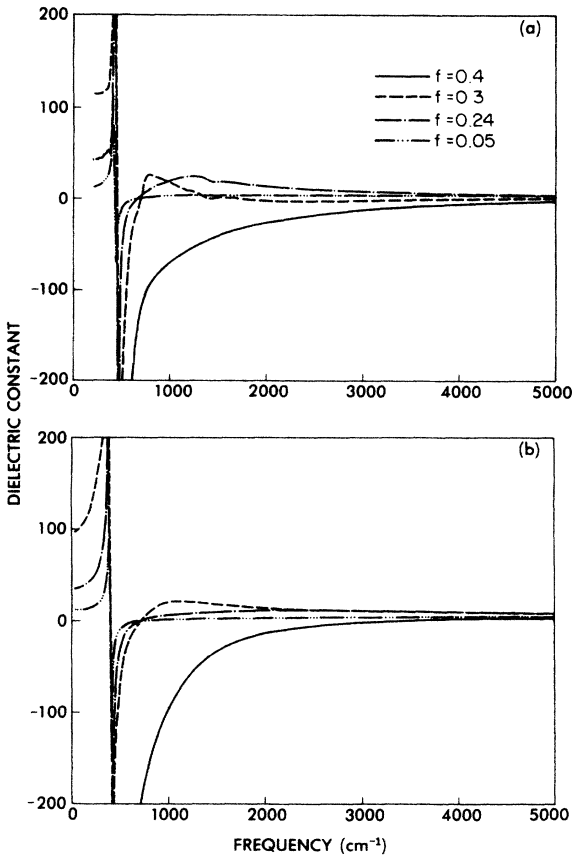

FIG. 8. (a) Real part of the dielectric constant obtained by Kramers-Kronig analysis of the reflectance of the Ni-MgO composites. (b) Real part of the dielectric constant calculated by the EMT.

The conductivity derived from the KKT also shows the percolation transition. As can be seen in Fig. 10(a), as the frequency decreases the conductivity for the samples with f below f_c approaches zero but the conductivity for the sample with $f=0.4$ ($>f_c$) diverges. For the $f=0.3$ sam-

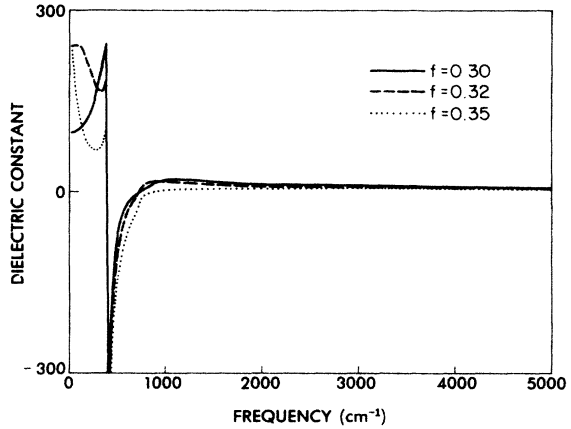

FIG. 9. Real part of the dielectric constant calculated by the EMT. This figure shows the changes of the dielectric constant near the percolation threshold.

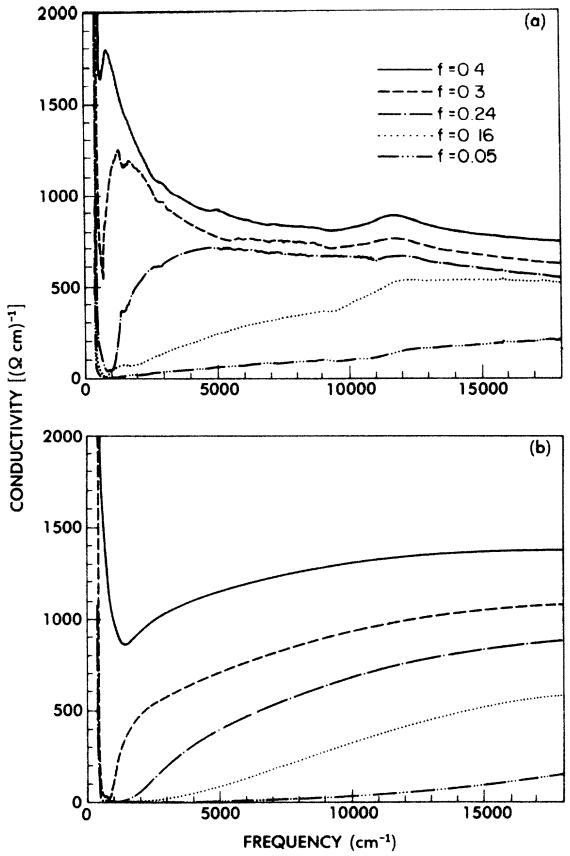

FIG. 10. (a) Frequency-dependent conductivity obtained by Kramers-Kronig analysis of the reflectance of the Ni-MgO composites. (b) Frequency-dependent conductivity calculated by the EMT.

ple, the decrease of the conductivity to zero at low frequencies is also masked due to the phonon bands located around 500 cm^{-1}. However, as the frequency decreases, the conductivity curve of the $f=0.3$ sample initially shows an increase for wave numbers below 5000 cm^{-1} but finally approaches zero below 400 cm^{-1}. Most of this percolation behavior can also be explained by the EMT. Comparison of Figs. 10(a) and 10(b) clearly indicates that the derived conductivity below $f=0.24$ qualitatively agrees with that of the EMT prediction. However, the behavior between 500 and 5000 cm^{-1} for samples of $f=0.3$ and 0.4 deviates from the prediction of the EMT.

Even though the EMT shows good agreement with our measured reflectance and the optical constants derived from the KKT, there exist at least three areas of concern. First, the sizes of the Ni particles were relatively large and do not satisfy the EMT approximation above the visible region. Secondly, the Drude formula for the dielectric constant of Ni, which we used by necessity in the EMT calculation, is not a good expression, since the interband transitions of Ni occur at 0.3 and 1.4 eV. Finally, the EMT is one of the simplest models that predicts the percolation transition and as such it only provides a qualitative description of percolation behavior.

V. CONCLUSIONS

We prepared a new granular metal system (Ni-MgO composites) by coprecipitation of NiO-MgO solid solutions and preferential reduction in a hydrogen atmosphere. Compared to the granular metal system prepared by cosputtering or coevaporation, these Ni-MgO composites were composed of larger metal particles without any oxide coating and had a different topology. This difference in topology and the lack of oxide coating on the metal particles resulted in a percolation threshold, $f_c=0.32\pm0.02$, which was much lower than that of the conventional granular metal system. Due to the differences in topology and their characteristics, the composites prepared by the coprecipitation and preferential reduction process provided a chance to extend the study of granular metal systems.

The reflection spectra of the Ni-MgO composites were measured and compared with the MGT and the EMT. The comparison of the spectra with the MGT and the EMT showed that our Ni-MgO composites can be better described by the EMT than by the MGT. The optical constants were derived by a Kramers-Kronig transformation, and they showed a qualitative agreement with the EMT. The high-frequency properties did not show the distinction between the samples below percolation and the one above percolation; however, in the low-frequency region, especially in the far-infrared region, most of the features of the percolation transition predicted by the EMT could be easily observed in the reflection spectrum and seen in the derived conductivity and the derived dielectric constant.

Note added in proof. In the calculation of the volume fractions reported in this paper, the void volume was not taken into account. If this void volume is included in the volume-fraction calculation, the percolation threshold (along with all other values of metal volume fraction) will be revised downward bringing it into closer agreement with theoretical predictions. The essential point of this paper, namely that the EMA better describes the behavior of granular metal composites (having the microstructure we used) is unchanged.

ACKNOWLEDGMENTS

We would like to thank John Golben for his comments on this manuscript. We are pleased to acknowledge Hendrik O. Colijn for his help on the transmission electron microscopy and C. Porter for providing us with his computer program of the Kramers-Kronig transformation. The financial support of the National Science Foundation through a grant to the Ohio State University Materials Research Laboratory (No. DMR 83-16989) and Grant No. DMR 84-05403 is gratefully acknowledged.

[1]J. C. Maxwell-Garnett, Philos. Trans. R. Soc. London **203**, 385 (1904); **205**, 237 (1906).

[2]The optical properties of "metal colloids" in ionic crystals were reviewed by A. E. Hughes and S. C. Jain, Adv. Phys. **28**, 717 (1979).

[3]A number of references may be found in S. D. Schwab, R. L. McCreery, and K. D. Cummings, J. Appl. Phys. **58**, 355 (1985).

[4]A number of references may be found in S. Norrman, T. Andersson, C. G. Granqvist, and O. Hunderi, Phys. Rev. B **18**, 674 (1978).

[5]R. W. Cohen, G. D. Cody, M. D. Coutts, and B. Abeles, Phys. Rev. B **8**, 3689 (1973).

[6]B. Abeles, H. L. Pinch, and J. I. Gittleman, Phys. Rev. Lett. **35**, 247 (1975).

[7]E. B. Priestley, B. Abeles, and R. W. Cohen, Phys. Rev. B **12**, 2121 (1975).

[8]J. C. C. Fan and P. M. Zavracky, Appl. Phys. Lett. **29**, 478 (1976).

[9]J. I. Gittleman, B. Abeles, P. Zanzucchi, and Y. Arie, Thin Solid Films **45**, 9 (1977).

[10]H. G. Craighead and R. A. Buhrman, Appl. Phys. Lett. **31**, 423 (1977).

[11]C. G. Granqvist and O. Hunderi, Phys. Rev. B **18**, 2897 (1978).

[12]C. G. Granqvist, J. Appl. Phys. **50**, 2916 (1979).

[13]U. J. Gibson, H. G. Craighead, and R. A. Buhrman, Phys. Rev. B **25**, 1449 (1982).

[14]U. J. Gibson and R. A. Buhrman, Phys. Rev. B **27**, 5046 (1983).

[15]J. Perrin, B. Despax, and E. Kay, Phys. Rev. B **32**, 719 (1985).

[16]T. Yamaguchi, M. Sakai, and N. Saito, Phys. Rev. B **32**, 2126 (1985).

[17]H. G. Craighead, R. Bartynski, R. A. Buhrman, L. Wojcik, and A. J. Sievers, Sol. Energy Mater. **1**, 105 (1979).

[18]D. Stroud, Phys. Rev. B **12**, 3368 (1975).

[19]D. M. Wood and N. W. Ashcroft, Philos. Mag. **35**, 269 (1977).

[20]J. I. Gittleman and B. Abeles, Phys. Rev. B **15**, 3273 (1977).

[21]I. Webman, J. Jortner, and M. H. Cohen, Phys. Rev. B **15**, 5712 (1977).

[22]D. Stroud and F. P. Pan, Phys. Rev. B **17**, 1602 (1978).

[23]D. Stroud, Phys. Rev. B **19**, 1783 (1979).

[24]P. Sheng, Phys. Rev. Lett. **45**, 60 (1980).

[25]P. Sheng, Phys. Rev. B **22**, 6364 (1980).

[26]G. W. Milton, Appl. Phys. Lett. **37**, 300 (1980).

[27]W. Lamb, D. M. Wood, and N. W. Ashcroft, Phys. Rev. B **21**, 2248 (1980).

[28]G. A. Niklasson, C. G. Granqvist, and O. Hunderi, Appl. Opt. **20**, 26 (1981).

[29]B. N. J. Persson and A. Liebsch, Solid State Commun. **44**, 1637 (1982).

[30]H. D. Park and E. R. Kreidler (unpublished).

[31]K. D. Cummings, J. C. Garland, and D. B. Tanner, Phys. Rev. B **30**, 4170 (1984).

[32]J. R. Jasperse, A. Kahan, J. N. Plendl, and S. S. Mitra, Phys. Rev. **146**, 526 (1966).

[33]H. Ehrenreich, H. R. Philipp, and D. J. Olechna, Phys. Rev. **131**, 2469 (1963).

[34]S. Roberts, Phys. Rev. **100**, 1667 (1955).

[35]L. R. Ingersoll, Astrophys. J. **32**, 282 (1910); A. Q. Tool, Phys. Rev. **31**, 1 (1910); J. R. Beattie and G. K. T. Conn, Philos. Mag. **46**, 1002 (1955); S. Roberts, Phys. Rev. **114**, 104 (1959).

[36]A complete historical review of this subject is given by Rolf Landauer, in *Proceedings of the First Conference on the Electrical Transport and Optical Properties of Inhomogeneous Media, Ohio State University, 1977,* edited by J. C. Garland and D. B. Tanner (AIP, New York, 1978), p. 2.

[37]D. A. G. Bruggeman, Ann. Phys. (Leipzig) **24**, 636 (1935).

[38]R. Landauer, J. Appl. Phys. **23**, 779 (1952).

[39]A number of articles and reference may be found in *Proceedings of the First Conference on the Electrical Transport and Optical Properties of Inhomogeneous Media, Ohio State University, 1977,* Ref. 36.

[40]F. Wooten, *Optical Properties of Solids* (Academic, New York, 1972).

[41]C. Kittel, *Introduction to Solid State Physics,* 5th ed. (Wiley, New York, 1976).

[42]I. Webman, J. Jortner, and M. Cohen, Phys. Rev. B **11**, 2885 (1975).

[43]D. Wilkinson, J. S. Langer, and P. N. Sen, Phys. Rev. B **28**, 1081 (1983); D. Stroud and D. Bergman, *ibid.* **25**, 2061 (1982); D. M. Grannan, J. C. Garland, and D. B. Tanner, Phys. Rev. Lett. **46**, 375 (1981).

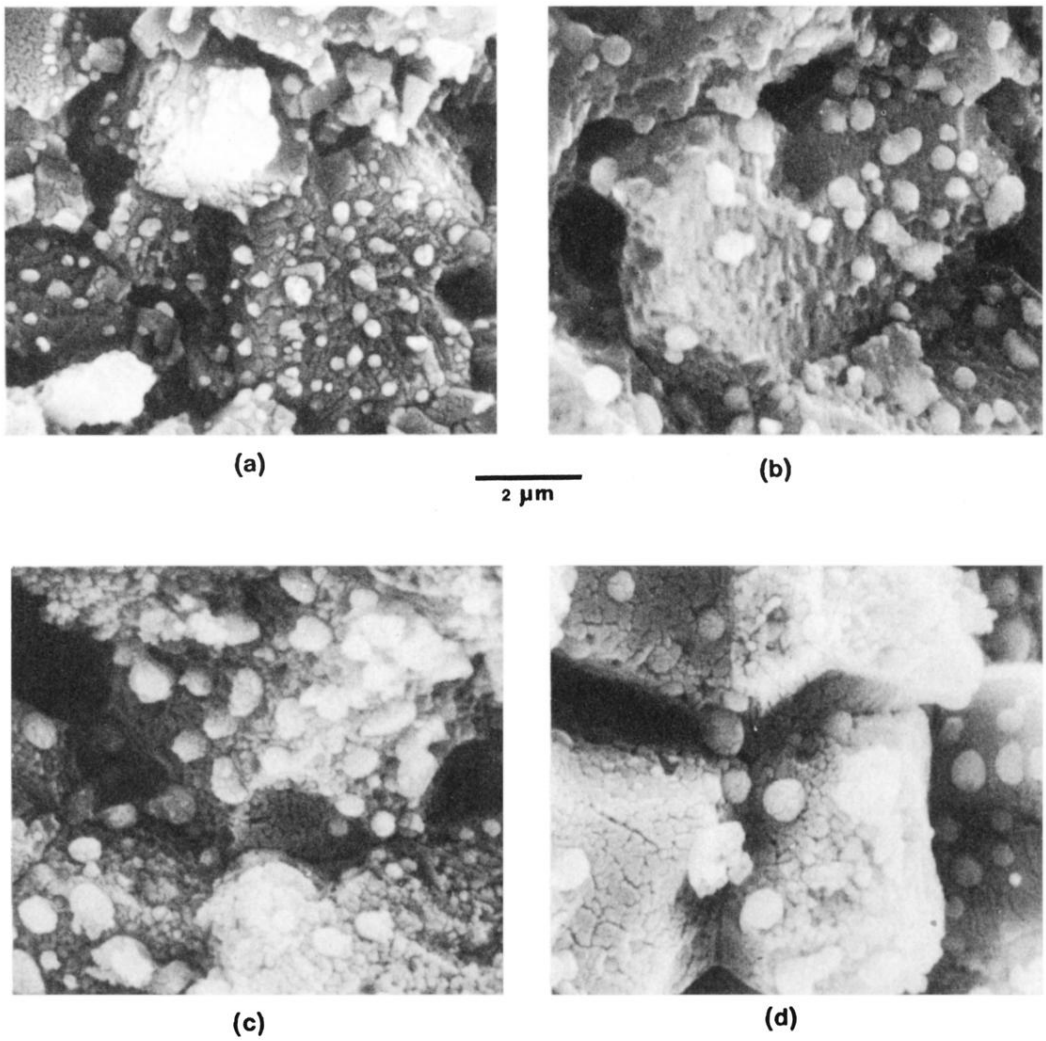

FIG. 1. Scanning electron micrographs of fractured surfaces of the Ni-MgO composites prepared by the coprecipitation of the NiO-MgO solid solutions and their reduction; (a) $f=0.1$, (b) $f=0.2$, (c) $f=0.3$, and (d) $f=0.4$.

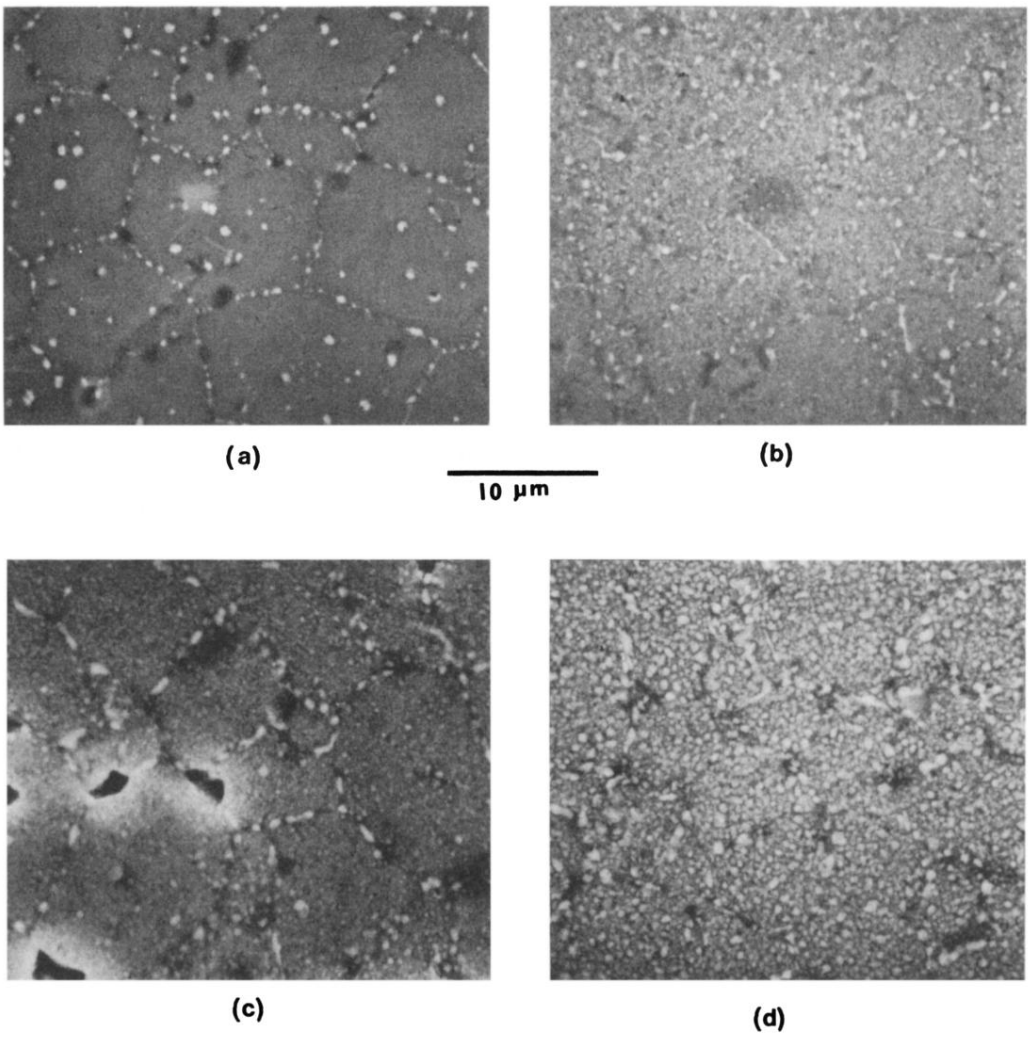

FIG. 2. Scanning electron micrographs of polished surfaces of Ni-MgO composites; (a) $f=0.05$, (b) $f=0.2$, (c) $f=0.3$, and (d) $f=0.4$.

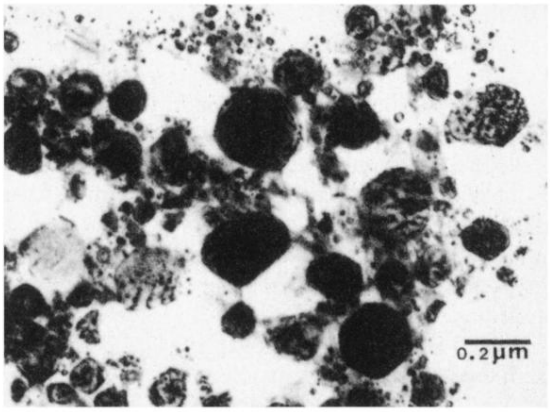

FIG. 3. Transmission electron micrographs of 30% Ni in an MgO sample.